Bedload fluxes in a glacier-fed river at multiple temporal scales

Velio Coviello[1,2], Gianluca Vignoli[3], Silvia Simoni[4], Walter Bertoldi[5], Michael Engel[2], Anuschka Buter[2], Giulia Marchetti[2], Andrea Andreoli[2], Sara Savi[6,2], Francesco Comiti[2]

[1] Research Institute for Geo-Hydrological Protection, CNR, Padova, Italy.

[2] Faculty of Science and Technology, Free University of Bozen-Bolzano, Italy.

[3] CISMA S.r.l., Bolzano, Italy.

[4] Mountain-eering S.r.l., Bolzano, Italy.

[5] Dipartimento di Ingegneria Civile Ambientale e Meccanica, Università degli Studi di Trento, Italy.

[6] Institute of Geosciences, University of Potsdam, Germany.

Corresponding author: Velio Coviello (velio.coviello@irpi.cnr.it)

Key Points:

- The power of the geophone-plate seismic signal better reflects the variability of bedload rate than the number of threshold-based impulses
- In glacier-fed mountain rivers bedload rates present large variability – up to four orders of magnitude – for the same flow discharge
- Bedload transport is controlled by summer rainstorm events superimposed on temperature conditions determining snow- and glacier melt

Abstract

In mountain rivers, long-term observations of water and sediment fluxes are crucial for understanding the dynamics of bedload fluctuations at multiple temporal scales. Here we analyze 7 years of data gathered at a bedload monitoring station in the glacier-fed Sulden/Solda River (South Tyrol, Italy). Continuous seismic data gathered from 8 geophone plates are analyzed to estimate the bedload flux at 1 minute scale. Sixty-five direct bedload sampling were carried out to derive the calibration equations adopted to quantify the transported bedload mass. The signal power is proposed as a more effective metric for calculating bedload mass than threshold-based impulses. Results show: (i) a remarkable variability of bedload rate for the same value of flow discharge; (ii) the joint effect of storm-driven flood events and seasonal changes in sediment supply on bedload rates; and (iii) the strong impact of climatic factors (i.e., temperature and snow cover) on bedload fluxes. Moderate bedload rates occurring in late spring/early summer are likely related to the mobilization of riverbed sediments, while higher bedload peak rates observed in July-August are associated with the activation of glacial and proglacial sediment sources. The dataset shows a complex climatic control on bedload transport at the basin scale, where precipitation, air temperature and snow cover determine flow and glacier melting dynamics. These findings suggest how the effects of the ongoing climatic change (e.g., higher frequency of intense rainfall events and prolonged heat waves) can result in a marked increase in bedload transport in glacier-fed rivers of the Alps.

Plain Language Summary

Water flowing in mountain rivers can transport a large amount of bedload, which is the coarse sediments that jump and roll on the river bed. The knowledge of the bedload flux matters for both ecosystems and human activities. Measuring how much bedload is transported is difficult as particles move below the water level. In this study we employ seismic sensors installed on the river bed to quantify the bedload transported by an Alpine river rising from a glacierized area. Moving particles produce ground vibrations that are more intense when the river transports more material. We found that the intensity of this “seismic noise” is extremely variable during the year and the river can rapidly become much more noisy in case of thunderstorms occurring during warm, summer periods. These findings are particularly relevant in the context of the ongoing global warming that is dramatically impacting on mountain areas where newly exposed stream reaches are emerging from the rapidly melting glaciers.

1 Introduction

In mountain rivers, bedload transport is the main driver of erosional/depositional processes and understanding its dynamics is crucial for the conservation of fluvial ecosystems, flood risk and hydropower management (Harrison et al., 2011; Lenzi et al., 2004; Rickenmann et al., 2016). The quantification of bedload fluxes is relevant for both ecosystems and human activities but is affected by large uncertainties. Traditional transport capacity-based equations assume that – at a given stable river cross-section – bedload transport rate is a function of the excess of a driving flow variable (e.g., dimensionless shear stress, unit discharge, unit stream power) with respect to the respective threshold value for sediment motion, which depends on both local flow and sediment properties (Bagnold, 1977; Einstein, 1950; Meyer-Peter and Müller, 1948). However, those equations are now known to largely overestimate the actual bedload rate in steep mountain rivers under ordinary flow conditions, due to both sediment supply limitations and form roughness (Barry et al., 2004; Comiti and Mao, 2012; Rickenmann, 2001; Schneider et al.,

2016). Indeed, different sediment supply regimes, runoff origin and history of flood events have a strong impact on bedload fluxes and make uncertainties in bedload prediction very large (Mao, 2012; Recking, 2012; Turowski et al., 2011).

Also, the long-established concept – initially proposed for low-gradient, transport-limited rivers – that ordinary floods (1-2 yr recurrence interval) are most effective in transporting sediments in the long-term than extreme, rare event for bedload transport (Wolman and Miller, 1960) has been challenged in steep channels (Lenzi et al., 2006). Thanks to the long-term bedload transport data collected in the Rio Cordon (Italian Alps, characterized by a nivo-pluvial hydrological regime) the latter authors showed how a single value of bedload effective discharge may be not applicable in such systems, and that floods larger than "bankfull events" may exert a stronger role than in lowland rivers.

Long-term (i.e., multi-annual) bedload monitoring is crucial to fill the large knowledge gaps still present about bedload dynamics, especially in supply-limited mountain rivers. Bedload monitoring based on geophone plates has been developed and applied for many years in Austria and Switzerland (e.g., Habersack et al., 2017; Rickenmann et al., 2012). Generally, geophone plate data are analyzed combined with direct bedload measurements to obtain calibration equations and to calculate bedload rates. Some information on the grain size distribution of bedload can be extracted from the geophone signal but uncertainties still exist, as confirmed by flume experiments (Wyss et al., 2016). Also, bedload transport during snow and glaciermelt periods has been identified by means of monitoring stations equipped with geophone plates (Rickenmann and Fritschi, 2017) but the role of climatic factors in controlling bedload yield at different temporal scales has been poorly investigated so far.

In glacier-fed rivers, climatic factors such as temperature and precipitation control the temporal and spatial evolution of sediment transfer by increasing sediment delivery from rockwalls and by modulating the remobilization of sediment from glacier forefields and rock glaciers (Etzelmüller and Frauenfelder, 2009; Kofler et al., 2021; Lane et al., 2017; Savi et al., 2021a). Deglaciation in particular is causing intense and widespread redistribution of sediment and that affects landscape stability and water quality and hence human health and livelihoods (Carrivick and Tweed, 2021). The current climate change, by increasing temperatures and intense rainfall events, poses an additional challenge in terms of management of extreme hydrological events and consequent morphological changes (Borga et al., 2014; Raymond Pralong et al., 2015; Rinaldi et al., 2015). Temperature conditions regulate the seasonal patterns of both water discharge and sediment transport by controlling the contributing drainage area and multiple processes such as glacier/snowmelt and permafrost thaw (Comiti et al., 2019; Li et al., 2021). To our knowledge, the effects of nivo-glacial regimes on effective discharge for bedload transport have not been explored yet using actual transport data.

In this paper, we analyze a 7-years dataset collected in the glacier-fed Sulden/Solda River (Italian Alps). Bedload fluxes in the study river are estimated by a novel approach to analyze the seismic signal detected by geophone plates. Indeed, the high-frequency seismic dataset allows us also to explore what signal parameters better predict bedload considering both ordinary and intense transport rates. After presenting the developed methodology for the extraction of information on bedload transport from geophone-plate data, the paper will address the following objectives: i) to analyze the temporal variability of bedload fluxes at different time scales (i.e., during single flood events as well as over different years); ii) to understand the role of climatic and geomorphic controls on bedload flux; iii) to determine the contribution of different water

discharges (and related runoff origin) in terms of cumulative bedload transport over the monitored period.

2 Materials and Methods

2.1 Study area

The study area is the Sulden/Solda river basin, located in the upper Vinschgau/Venosta Valley (eastern Italian Alps) and belonging to the Adige river basin (Figure 1a). The Sulden basin drains about 130 km² at the outlet defined by the location of the monitoring station located at Stilfserbrücke/Ponte Stelvio, Autonomous Province of Bozen/Bolzano. The basin can be subdivided into the actual Sulden and the Trafoi sub-catchments, that measure 75 and 51 km² respectively (i.e., there are about 5 km^2 which drain below the Sulden-Trafoi confluence, Engel et al., 2019; Buter et al., 2020).

The Sulden basin (Figure 1b) is characterized by a high topographic relief, ranging from around 1100 m a.s.l. at the outlet of the basin to 3905 m a.s.l. corresponding to the Ortler/Ortles peak, the highest mountain of the Eastern Alps. In 2016, the area covered by glaciers in the Sulden basin was around 18 km² (Autonomous Province of Bozen-Bolzano, 2017), representing the 14% of the total basin area. The presence of glaciers (both debris-covered and clean ice), proglacial landforms and extensive talus cover, combined with the high energy relief of the basin, results into complex and fast-evolving dynamics of sediment transfer (Buter et al., 2020). The upper basin hosts an automatic weather station (AWS) located at an altitude of 2825 m a.s.l. (Madritsch/Madriccio station, run by the Meteorological Office of the Autonomous Province of Bozen-Bolzano). The Madritsch AWS records solar radiation, snow depth, and air temperature at 10 min intervals and precipitation at 5 min intervals.

The bedrock geology of the Sulden basin includes metamorphic rocks of the Ötztal- and the Campo-Crystalline (mainly composed by quartz phyllites, mica schists, and ortho- and paragneiss) and Permo-Triassic sedimentary carbonate rocks (Buter et al., 2020). Metamorphic rocks crop out in the eastern slopes of the Sulden sub-catchment, where they belong to the Permian orthogneisses of the Lasa unit, and western slopes of the Trafoi sub-catchement. Limestones and dolomites dominate in the Trafoi sub-catchment, but are also exposed in the western side of the Sulden sub-catchment, at high elevation on the Ortler massif (Figure 1b). The Sulden River has a nivo-glacial regime, characterized by the minimum and maximum runoff in winter and in summer, respectively. Snowmelt runoff dominates in May and June, whereas the glacier-melt period typically spans from July to late August- early September (Engel et al., 2019a). For the climatic period 1981–2010, mean annual air temperature (MAAT) at Madritch AWS was -2.4°C, whereas mean annual precipitation (MAP) averaged 980 mm (Savi et al., 2021; 3PClim database).

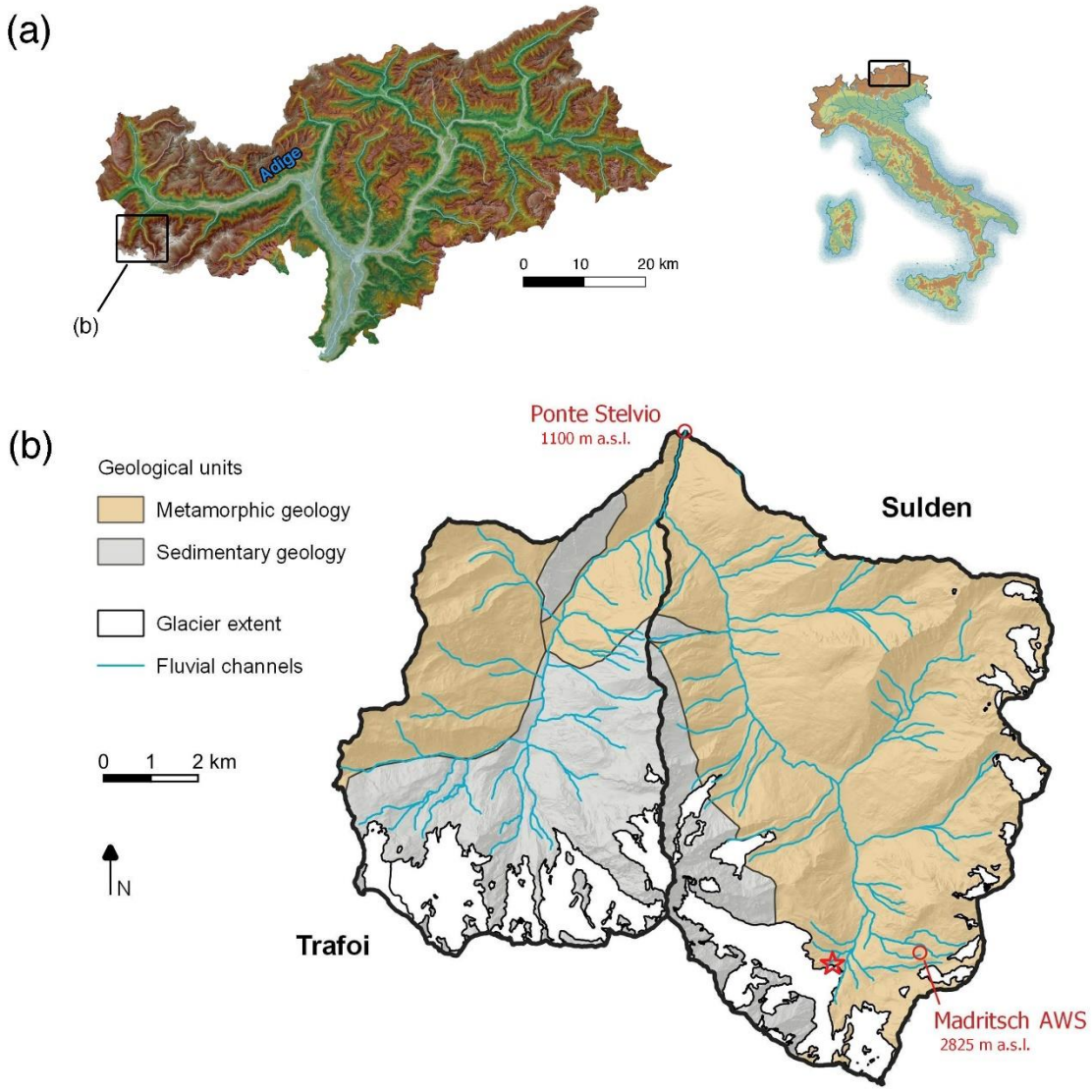

Figure 1 - Location of the Sulden/Solda and Trafoi catchments in the Vinschgau/Venosta Valley, Province of Bozen-Bolzano, Italy; (b) simplified geomorphic map of Sulden basin at the outlet defined by the village of Stilfserbrücke/Ponte Stelvio, where the monitoring station is located. The red star indicates the Sulden glacier front (see pictures at Figure 14).

2.2 Continuous water and bedload monitoring

The monitoring station of Stilfserbrücke – Ponte Stelvio was designed to monitor both water and sediment fluxes (Figure 2). The construction and management of this station was the result of the cooperation between public institutions (Universities and local agencies) and private companies (Vignoli et al., 2016). At the station, suspended sediment transport is also measured by means of a turbidimeter (Engel et al., 2019a). In this work, we focus on bedload transport only, which is indirectly monitored by a rack of eight geophone plates, installed on the downstream end of a check dam (Figure 2a). The rack is 4-m long and covers half of the river width (8 m) from the mid-channel to the right bank (Figure 2b) and is fixed on a concrete structure with a cantilever metal structure. Water level is measured at 10 min intervals and water discharge is calculated

using a flow-rating curve calibrated by means of twenty-seven direct discharge measurements ranging from 1 to 20 m^3/s and performed in 2014 and 2015 using the salt dilution method. The geophones are mounted on the underside of a 0.358-m long, 0.494-m wide, and 0.01-m thick steel plate. Each plate is seismically isolated from the frame and the rack using elastomer elements. During bedload transport, gravel particles slide, roll or saltate over the steel plate. The geophone contains a magnet in a coil that acts as an inductive element. The plate transmits to the geophone sensor the vibration generated by bedload transport and, thereby, an electrical current proportional to the velocity of vibration is produced by electromagnetic induction inside the geophone. When the voltage exceeds a preselected very-low amplitude threshold, A_{min}, the raw seismic signal sampled at 5 kHz is recorded.

Data recording started on 29 April 2014 and stopped on 6 November 2020. Some gaps affect the time series, especially in 2016, 2018, and 2019 due to technical problems (Table 1). In this paper, from 2014 to 2020 we focus on the period May-October (six months), during which most bedload transport occurs.

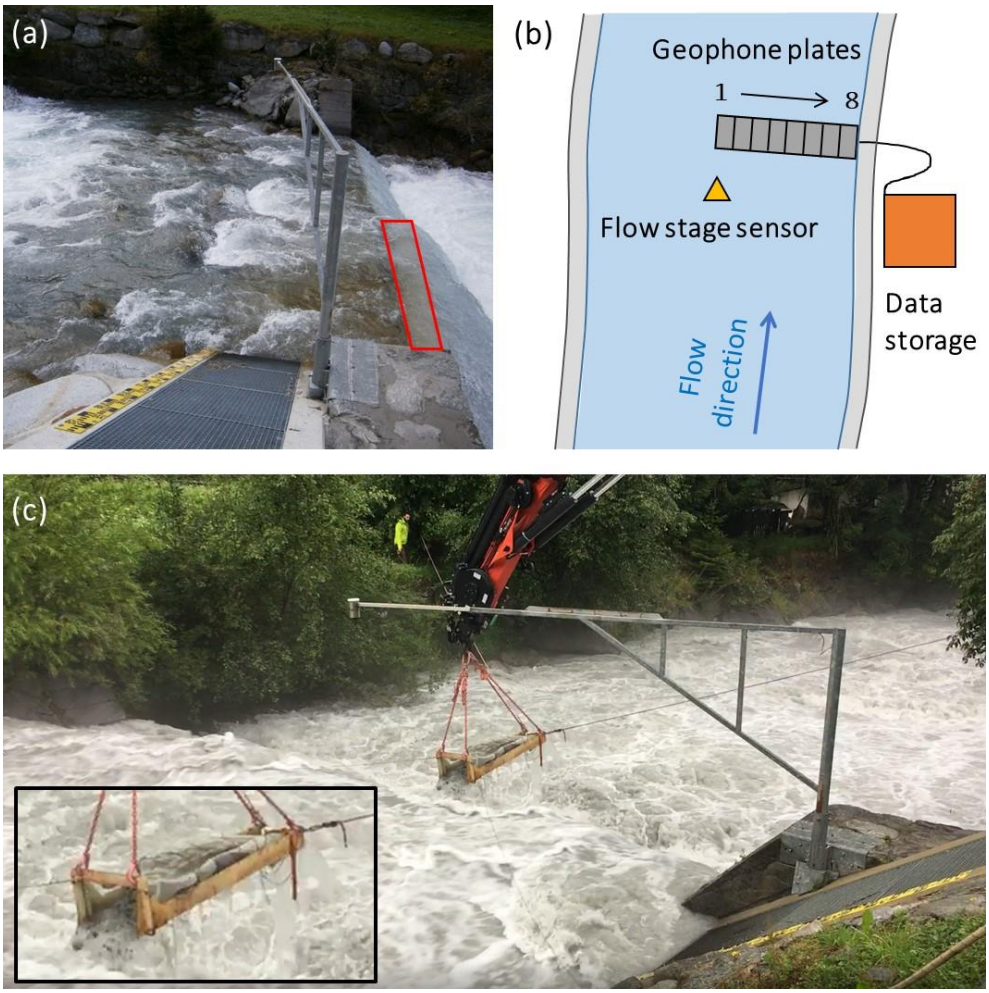

Figure 2 - The Stilfserbrücke – Ponte Stelvio monitoring station on the Sulden-Solda River: (a) the check dam instrumented with the rack of geophone plates (red frame); (b) sketch of the monitoring station; (c) direct measurement with the portable trap (7 August 2019).

2.3 Direct bedload measurements

Direct bedload measurements were performed using a portable bedload trap made by a net with opening size of 3.6 mm, anchored to a metal frame and handled by a crane (Figure 2c). The sampling duration varies from 1 to 10 minute, depending on the bedload transport intensity. During each measurement, the trap was inserted into the stream flow right downstream of a plate and held by a crane and four ropes, which helped to keep the trap stable at the sampling position. The sampling position was variable over the eight geophone plates (Table 2). We sieved the collected material (i.e., sediment particles larger than 3.6 mm in diameter, d) on site using four sieves with opening size of 64 mm, 45 mm, 32 mm and 22 mm. The four separated sample classes (d > 64 mm, 64 > d > 45 mm, 45 > d > 32 mm, 32 > d > 22 mm) and the finest fraction (d < 22 mm) were weighted and then released back into the stream. We obtained the rating curves for bedload coupling the bedload direct measurements with the seismic information and the resulting power law regressions are presented in the shape:

$$Q_{btrap} = ax^b \quad (1)$$

where x represents a metric of the seismic signal (see section 2.3) and Q_{btrap} the bedload rate at the reference plate (kg min^{-1}). In Table 2, the list of direct bedload measurements is reported. The minimum and the maximum measured value of Q_{btrap} are 0.27 kg min^{-1} (25 June 2020) and 54.35 kg min^{-1} (7 August 2019).

2.4 Processing of geophone plate data

Data gathered at the geophone plates are sampled at 5 kHz and recorded continuously. A detection algorithm based on an intensity-duration (I-D) threshold together with a Portable Network Graphics (PNG) compression allow the recording of the raw signal. A very low I-D threshold activates the recording of the signal while below that threshold zero values are saved (i.e., no transport). The raw signal is then compressed in PNG files that contain about 7 minutes of signal each and occupy from few hundreds of KB to few MB, see supplementary material for details. This approach allows the storage of one year of 5 kHz data in about 20 GB of disk space per plate, see supplementary material for details. The saved data can be elaborated counting the number of impulses above a given threshold (i.e., the "traditional" geophone plate signal elaboration described in Rickenmann et al., 2014) and applying any type of signal processing. We extracted three basic signal metrics from the raw signal, calculated over a 1-min time window: the maximum amplitude A_{max}, the number of impulses Imp, and the signal power P (Figure 3).
The transformation into impulses consists in counting how many times the signal exceeds a threshold after crossing the horizontal axis in a given time period (Figure 3a). Assuming a constant flow velocity, the energy transfer from the sediments to the plates is controlled by the sediment concentration, the grain size, and the flow turbulence (Coviello et al., 2018; Gimbert et al., 2014; Turowski et al., 2015). We used four different thresholds (0.01, 0.04, 0.16, 0.32 V) as the signal intensity depends on the energy transfer from the flow to the plate. The number of impulses recorded in a given time period is threshold-dependent. The need to select the threshold value represents a possible drawback of such an approach because (i) it is site dependent and (ii) it should be adapted to transport conditions. These limitations have been already observed in the field of debris flow monitoring, where the impulses have been also employed in the past (Arattano et al., 2014). The values of A_{max} are computed as the maximum amplitude reached by the raw signal

during the sampling interval (Figure 3a). The signal power P (Figure 3b) is calculated over a time window of 1 minute by using the following formula, where $T = 1min$:

$$P = \frac{1}{T}\int_{t_1}^{t_2} |u(t)|^2 \, dt \quad (2)$$

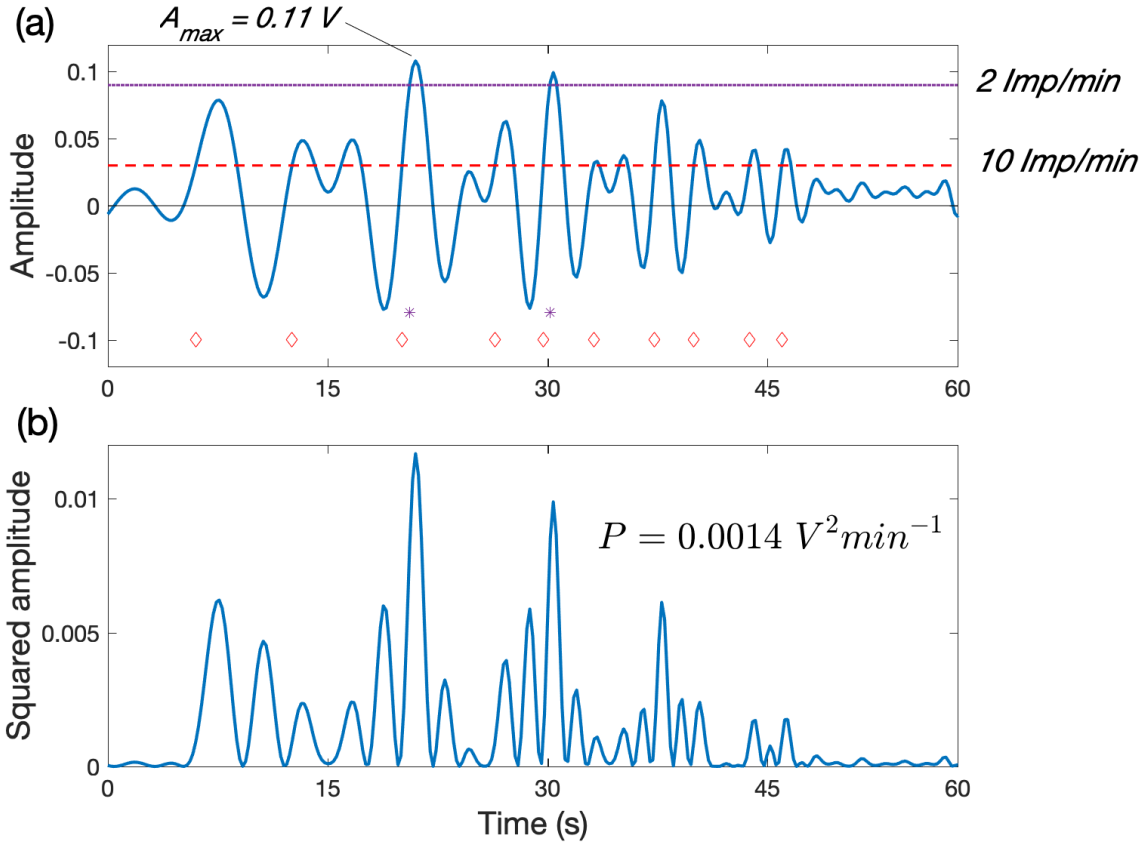

Figure 3 – Extraction of the main signal metrics from the raw seismic signal: (a) maximum amplitude (A_{max}) and impulses per minute calculated with two thresholds (i.e., violet and red dashed lines). Violet stars and red diamonds represent the Impulses counters for the two different thresholds. (b) Signal power (P) calculated summing the squared amplitude values over a time window of 1 minute (see eq. 2).

2.5 Effective discharge

The availability of both water and bedload monitoring data at the minute-scale resolution allowed us the quantitative investigation of flow conditions that are more effective for bedload transport. The effective discharge is defined as the flow rate that is most effective in the long-term transport of sediment (Wolman and Miller, 1960), and thus the effective discharge is a function of both the intensity and the frequency of occurrence of flow conditions transporting sediments. Building upon this concept, Lenzi et al. (2006) applied a data-driven method to calculate the effective discharge curve for bedload transport E_b based on the average bedload rate measured - and not estimated by transport capacity equations or bedload rating curves, as most commonly done - for each flow class:

$$E_b = Q_b * f \quad (3)$$

where Q_b is the bedload rate (kg/min) and f the flow frequency (%). The flow class associated to the maximum value of E_b indicates the effective discharge for bedload during the monitored period. In this work, we adopt this method to analyze the 7-years bedload dataset collected in the Sulden River, adopting flow class intervals of 4 m^3 s^{-1}.

3 Results

3.1 Direct bedload measurements

From 2014 to 2020, 76 direct bedload measurements by the crane-suspended trap were carried out, but only 65 of them were used for calibration after a validation of the dataset. Data validation consisted in eliminating the samples affected by clear problems encountered during the measurements (e.g., unstable trap or seemingly positioned onto the geophone plates) or that represented outliers in the distribution of paired value of extracted mass vs the signal metrics described below. In total, about 2068 kg of bedload were used to derive the calibration functions after this validation procedure (about 86% of the total sampled mass, i.e. 2412 kg).

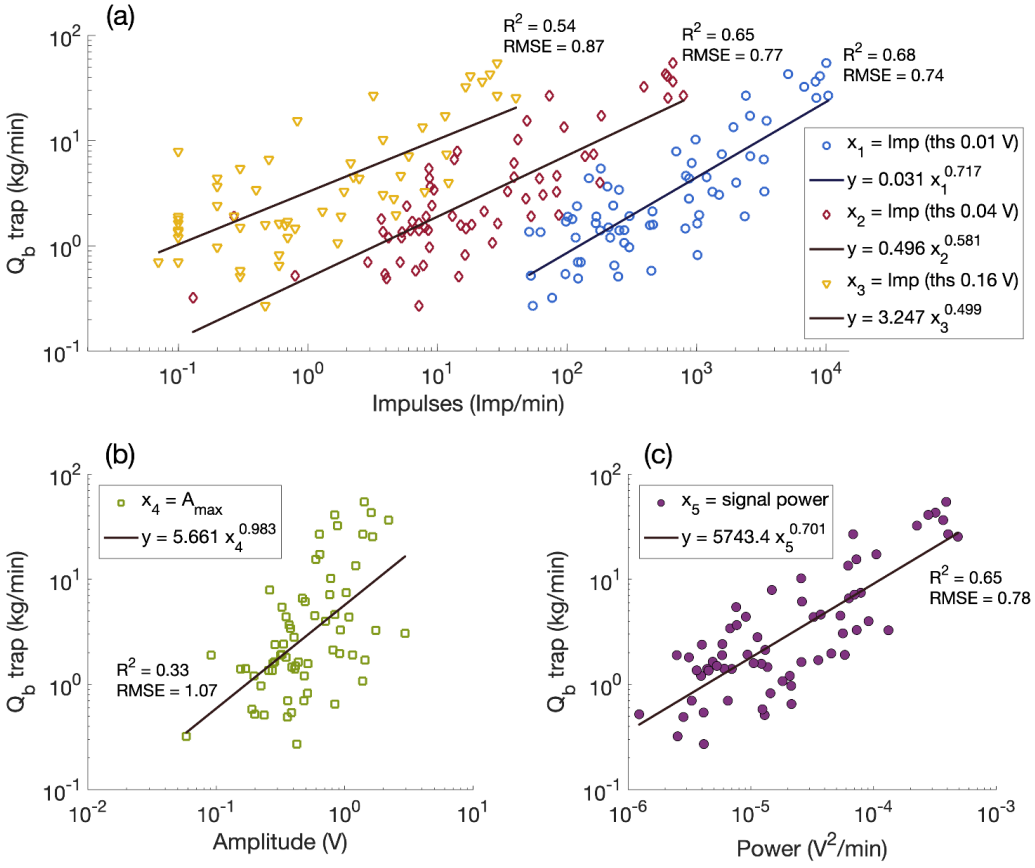

Figure 4 – Geophone plate calibration relationships of the bedload rate as a function of (a) the Impulse rate calculated with three different thresholds, (b) the maximum amplitude and (c) the signal power normalized per minute. For each equation, the coefficient of determination (R^2) and the Root Mean Square Error (RMSE) are reported.

The three signal metrics employed for calibration are (i) impulses, (ii) maximum amplitude and (iii) the signal power (Figure 4). We extracted the Impulses per minutes using four different thresholds and we divided the sampled weight and the number of impulses by the sampling duration to obtain the bedload rate (kg min^{-1}) and the Impulse rate (Imp min^{-1}). Then, each pair of values is plotted (Figure 4a). A lower threshold (i.e., 0.01 V) leads to a higher number of impulses. Raising the threshold, the number of impulses tends to decrease and progressively some data points disappear from the plot. For this reason, we selected three thresholds to be tested for calibration (0.01, 0.04, 0.16 V) and we do not present the analysis of impulses related to the highest threshold (0.32 V), which also presents large data scattering. The lowest threshold produces a number of impulses featuring the highest correlation coefficient and the lowest error when a power law regression is applied (Figure 4a). The regressions of A_{max} and of the signal power P are reported in Figure 4b and Figure 4c, respectively. In Figure 4, the coefficients of determination and the prediction errors of the different regression equations are reported. The p-values of all equations are < 0.001.

Figure 5 shows the - relatively small - coarsening of the bedload grain size distribution (GSD) with increasing flow discharge. The GSD of 57 measurements out of 65 is presented in three classes of discharge: 6.5-12 (low), 12-15 (medium), and 19-21 m^3/s (high). In general, a larger discharge results in coarser transported bedload material, as a consistent pattern among the three discharge classes is visible that shows higher quantiles associated to larger flow. An exception is represented by sediments with d < 22 mm, for which the medium discharge class features the highest proportion.

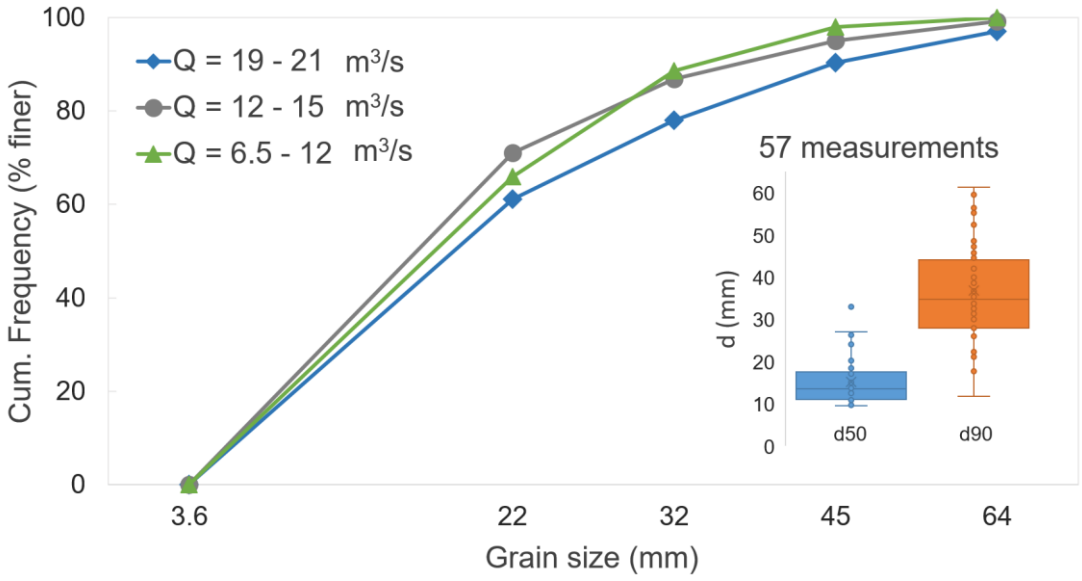

Figure 5 – Grain size distributions (GSD) of bedload transport measurements taken by the portable trap. For better visibility of trends, the grain size distributions are presented for classes of discharge. In the inset, boxplots representing the distribution of d50 and d90 for the available GSD dataset (57 bedload measurements out of 65).

3.2 Estimation of bedload yield

In Figure 6, we show the annual bedload yield (d > 3.6 mm) at Stilfserbrücke calculated using the three calibration equations described in section 3.1, which are based on different signal

metrics (impulses, maximum amplitude and signal power). For impulses, we selected the calibration equation based on the impulses calculated with a threshold value of 0.01 V given its higher correlation coefficients. Data gaps on single plates were filled using data collected on neighboring plates in order to deliver homogenous annual values (Figure 6). Linear interpolation was used to estimate the bedload mass in case of data gaps, with a correcting factor of 0.7 going from center to right bank. The correcting factor was calculated based on the bedload attenuation profile observed at the monitoring station. For three years (2016, 2018, and 2019) it was not possible to fill some data gaps occurred in summer on all geophone plates (Table 1). Because only half of the monitored river cross-section is equipped with geophone plates, the final bedload mass was obtained doubling the calculated values by assuming a symmetrical distribution of bedload transport across the section. Such an assumption is considered sufficiently valid due to the straight, engineered geometry of the Sulden channel upstream and downstream of the monitored section.

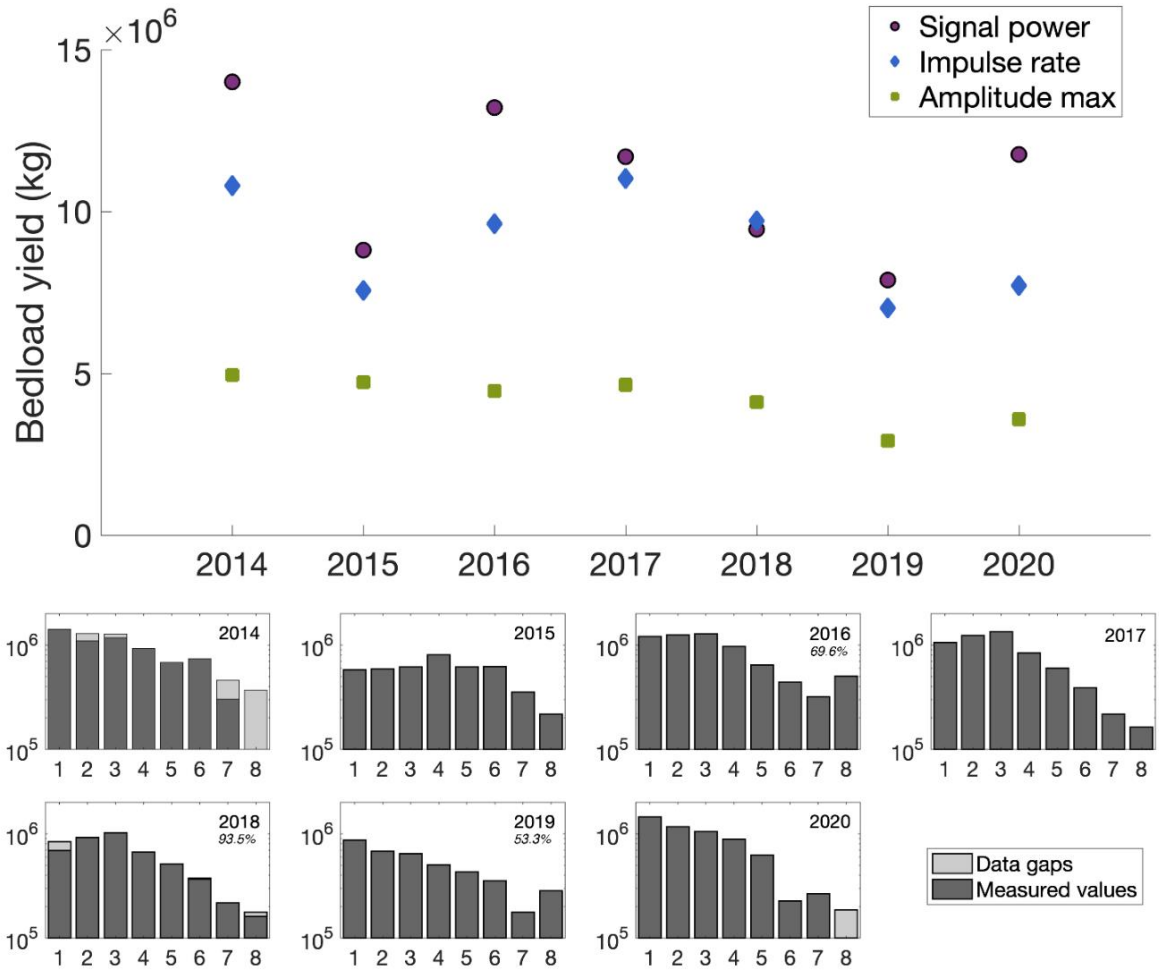

Figure 6 – Annual bedload yield (kg) from 2014 to 2020 calculated using three calibration equations based on signal power, impulses calculated with a threshold of 0.01 V and maximum amplitude. Some years are affected by important data gaps in June and July (28 days in 2016, 6 days in 2018 and 43 days in 2019). Bar plots report annual yield at each plates (1 = central plate, 8 = plate bordering the right bank) each year. Percentages indicate the completeness of the dataset, when the value is not indicated it means 100%.

The calibration equation based on the maximum amplitude underestimates bedload transport while the two other equations (impulses and signal power) return comparable values. However, there are specific years (i.e., 2014, 2016, and 2020) where the two parameters differ significantly (Figure 6). These latter years are characterized by intense bedload events and – similarly to what has been observer for the maximum amplitude – it looks like the number of impulses is damped and therefore it is not optimal to characterize the full range of bedload variability observed here. More details on the analysis of these two parameters are reported in the discussion section. Hereinafter, the bedload rate at one single plate Q_b (kg min^{-1}) is calculated by means of the signal power (P) equation:

$$Q_b = 5743.4P^{0.701} \qquad (4)$$

and the bedload concentration C_b (kg/m^3) at the whole cross-section (8-m wide) as:

$$C_b = \frac{16Q_b}{Q} \qquad (5)$$

3.3 Continuous bedload transport data and hydro-meteorological variables

In Figure 7, the water discharge and unit bedload rate measured at the Stilfserbrücke station are shown for the whole monitoring period, along with hydro-meteorological data (daily precipitation and mean air temperature) and snow cover measured at the Madritsch AWS.

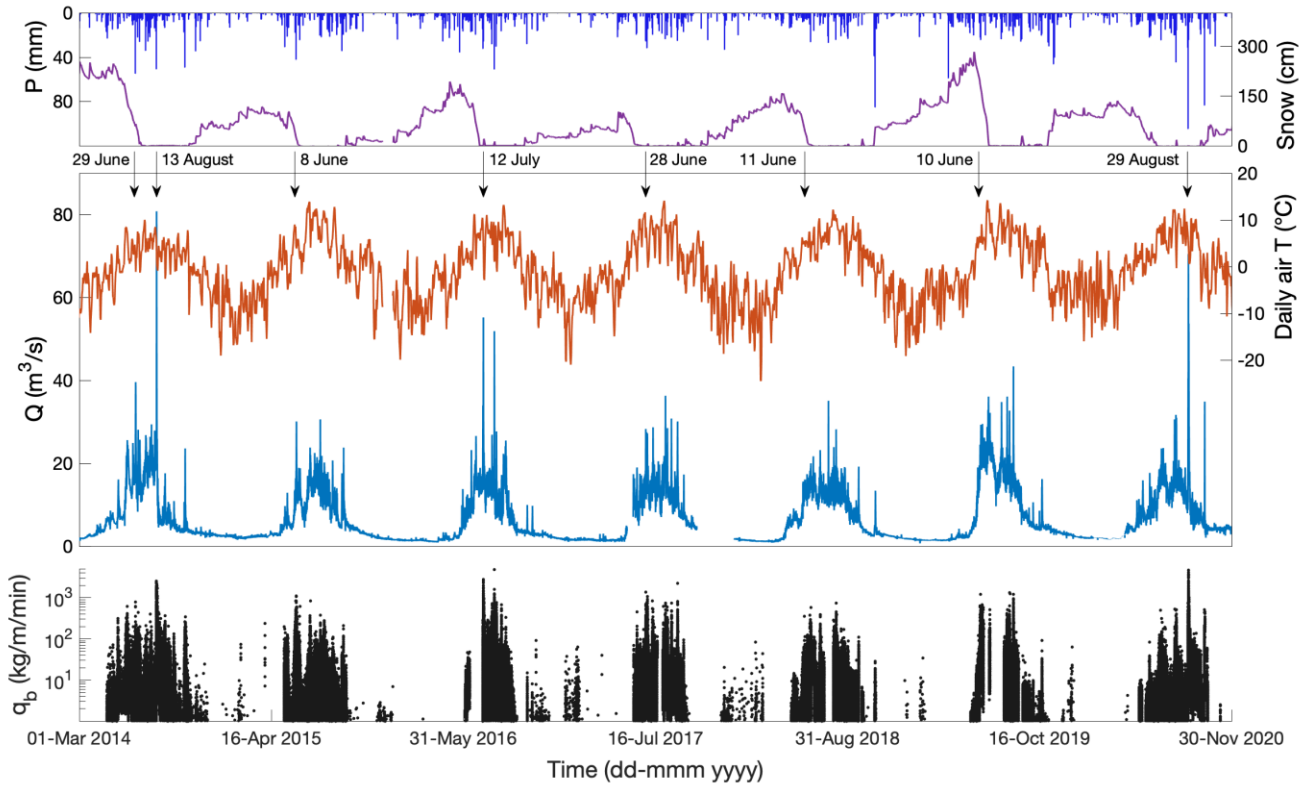

Figure 7 – Hydro-meteorological data from the Madritsch AWS (precipitation, snow depth, air temperature) and flow discharge and unit bedload rate (at plate 1) measured at Stilfserbrucke from 2014 to 2020. Some events investigated in detail in this work are marked with black arrows.

For sake of simplicity, here the unit bedload rate q_b is calculated using data collected at plate 1 only, applying equation 4. The seasonal variability of hydro-meteorological variables is well visible together with short-scale fluctuations due to intense rainfall events and snow-melt periods in late spring/early summer. Water discharge ranges from values of about 5 m^3 s^{-1} before and 30 m^3 s^{-1} during the snow- and glacier-melt periods. Peak values of flow discharge higher than 40 m^3 s^{-1} correspond to few flood events. As expected, the most important peaks in water discharge and unit bedload rate occurred during the same events (e.g., 13 August 2014, 12 July 2016 and 29 August 2020), however, unit bedload rates show a remarkable variability of more than three orders of magnitude.

By using the Lenzi et al. (2006) approach (section 2.5), the average bedload transport rate (kg min^{-1}) associated with each flow class was calculated (Figure 8a), and the value of E_b for each flow class – resulting from the multiplication of the actual flow frequencies and mean bedload rates measured at the station – could be calculated (Figure 8b). Interestingly, the E_b curve does not present a single relative maximum, but instead presents three relative peaks, respectively at about 18, 42 and 70 m^3 s^{-1}. The physical interpretation of such a complex pattern for the E_b curve – and of its peak values – will be presented in the discussions.

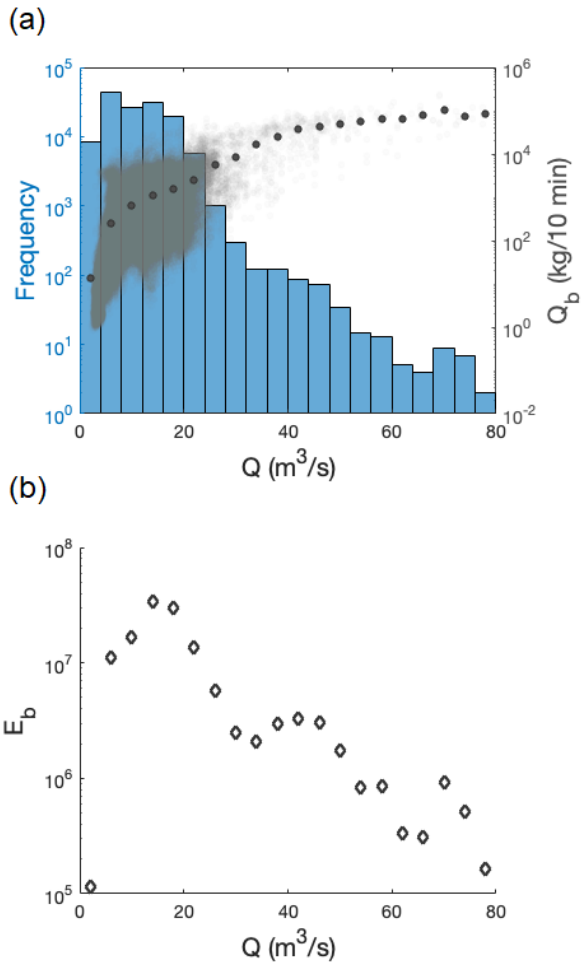

Figure 8 - Combined plot of flow frequencies and associated bedload rates (a, larger dots represent mean bedload rates for each class) and the resulting product of the two variables (E_b values, b) as determined from data collected at the Stilfserbrücke station for the 2014-2020 period. The shaded area in (a) represents the entire dataset of bedload rates.

3.4 Analysis of the variability of bedload transport

Bedload rate was analyzed in comparison with the flow discharge to investigate the impact of other factors than runoff, i.e. sediment supply, on bedload transport. For each year, one reference plate was selected based on two criteria that are (i) the completeness of the monitoring dataset and (ii) the maximum bedload yield measured at the instrumented cross-section (see bar plots in Figure 6). The bedload rate Q_{bn} at selected reference plate n was calculated by means of the power rate equation, as described in the previous section. Results show a remarkable variability of bedload concentration $C_b$through time. Highest values of bedload concentration C_b are usually observed in July and August (Figure 9) but the trend is irregular. In particular, 2014 and 2020 feature two bedload events that dominate the distribution. Other years, such as 2017 and 2018, do not present intense events but a moderate and regular bedload transport from early June to the end of August.

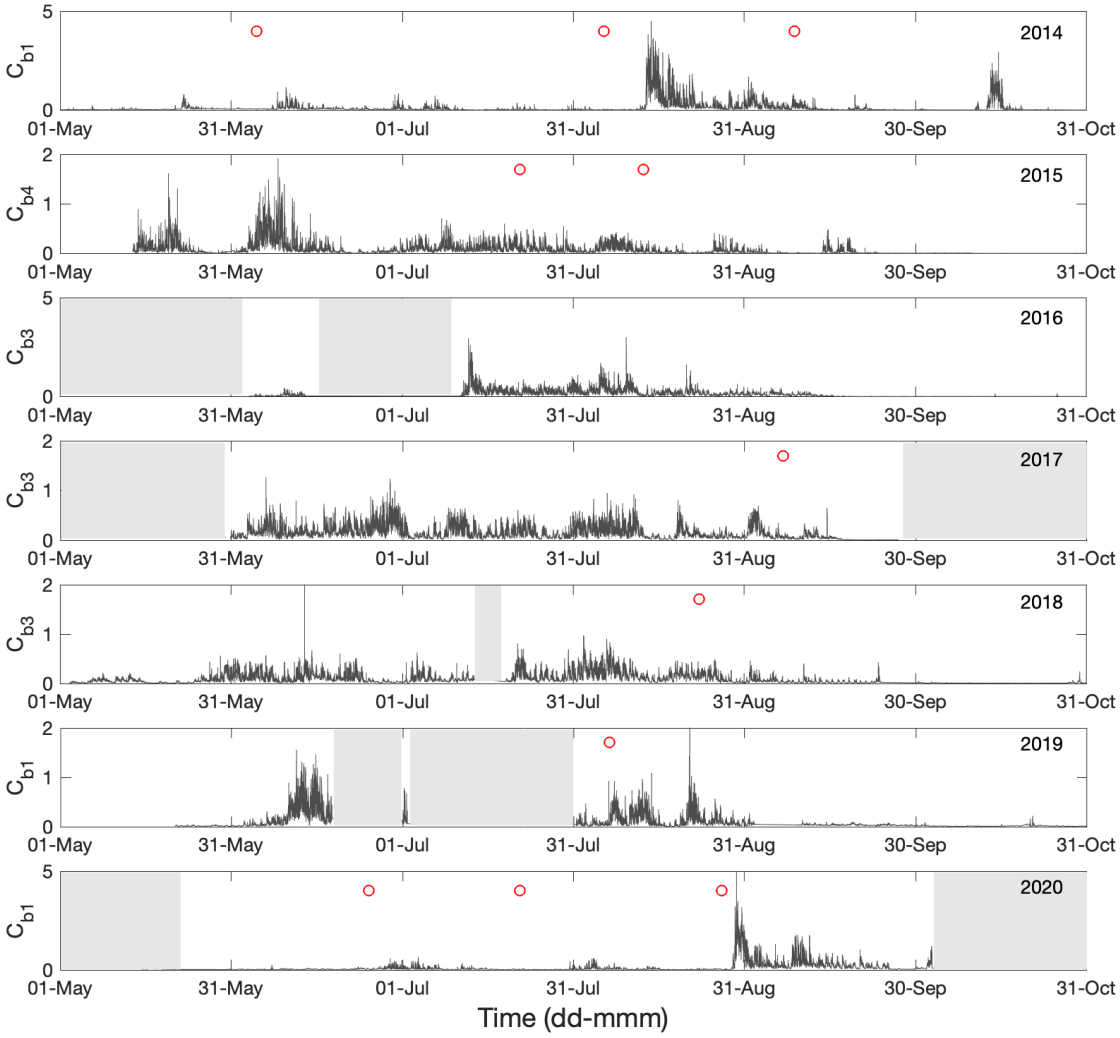

Figure 9 – Bedload concentration (kg/m³) measured from 2014 to 2020 at the Stilfserbrücke station. C_b is calculated using data from plate 1 in 2014, 2019 and 2020, plate 4 in 2015 and plate 3 in in 2016, 2017 and 2018. Grey areas represent data gaps in the seismic recordings. Red circles in indicate days during which direct measurements were performed (see section 2.3).

In Figure 10, we analyze in detail one single year, the 2014, presenting a complex seasonal trend. We used data gathered at plate 1 to draw the figure, as they are representative of the maximum bedload rate observed at the cross-section. In Figure 10a, the temporal evolution of C_b^* from 1 May to 31 October 2014 is plotted together with the daily precipitation in the upper Sulden basin (data from Madritsch AWS). The maximum bedload concentration is reached on 13 August 2014, when a large flood event was triggered by a precipitation event that featured a cumulated rainfall of 50.9 mm in 24 hours. In the scatter plot (Figure 10b) the measured values of bedload rate are aggregated at 10-min time intervals (i.e., the recording frequency of the flow stage sensor) and grouped in three classes: May-June, July-August and September-October. The first class (late spring/early summer) features an increasing trend both in bedload rate of two orders of magnitude, the second class (warmer summer weeks) is characterized by the largest bedload variability of four orders of magnitudes, and the third class (late summer) shows a decreasing trend of bedload rate. A similar seasonal trend is observed in the following years (see supplementary material).

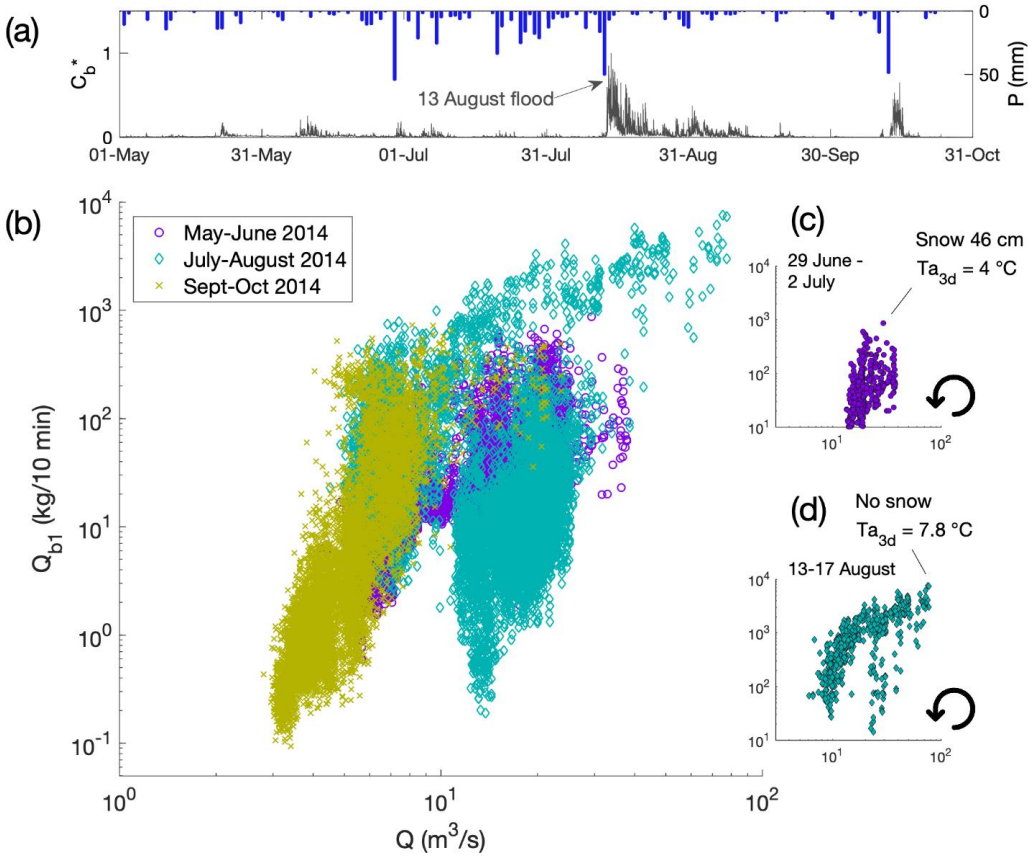

Figure 10 - (a) Bedload concentration (normalized) at the Stilfserbrücke station and daily precipitation at Madritsch AWS from 1 May to 31 October 2014. (b) Scatter plot of bedload rate measured at plate 1 vs the total discharge. The insets provide details on two flow events that occurred on 29 June (c) and 13 August (d). Snow cover and the mean air temperature are calculated on data gathered at Madritsch AWS.

The flood event occurred on 13 August 2014 transported about 4,500 tons of bedload in 96 h (30% of the annual transport), featuring a bedload peak of 10^4 kg in 10 min. In mid-August, there was no snow cover in the upper basin. On August 13, the mean air temperature calculated on the

previous seven days Ta_w was 7.1 °C and the mean air temperature calculated on the previous 3 days Ta_{3d} was 7.8 °C. In the following three days, the bedload rate remained quite intense, ranging from 10^2 to 10^3 kg in 10 min while flow discharge decreased from 80 m^3/s to about 10 m^3/s, inducing a counterclockwise hysteresis cycle (Figure 10c). A very similar precipitation event that occurred on 29 June 2014 (54.9 mm in 24 hours) produced a bedload event with a peak value of 10^3 kg in 10 min (Figure 10d), one order of magnitude lower than the one occurred on 13 August 2014. Indeed, the precipitation event of 29 June 2014 did not result in a significant response in terms of bedload yield as it occurred under very different weather conditions ($Ta_w =$ 3.9 °C and 46 cm of snow cover) that likely impeded particle motion.

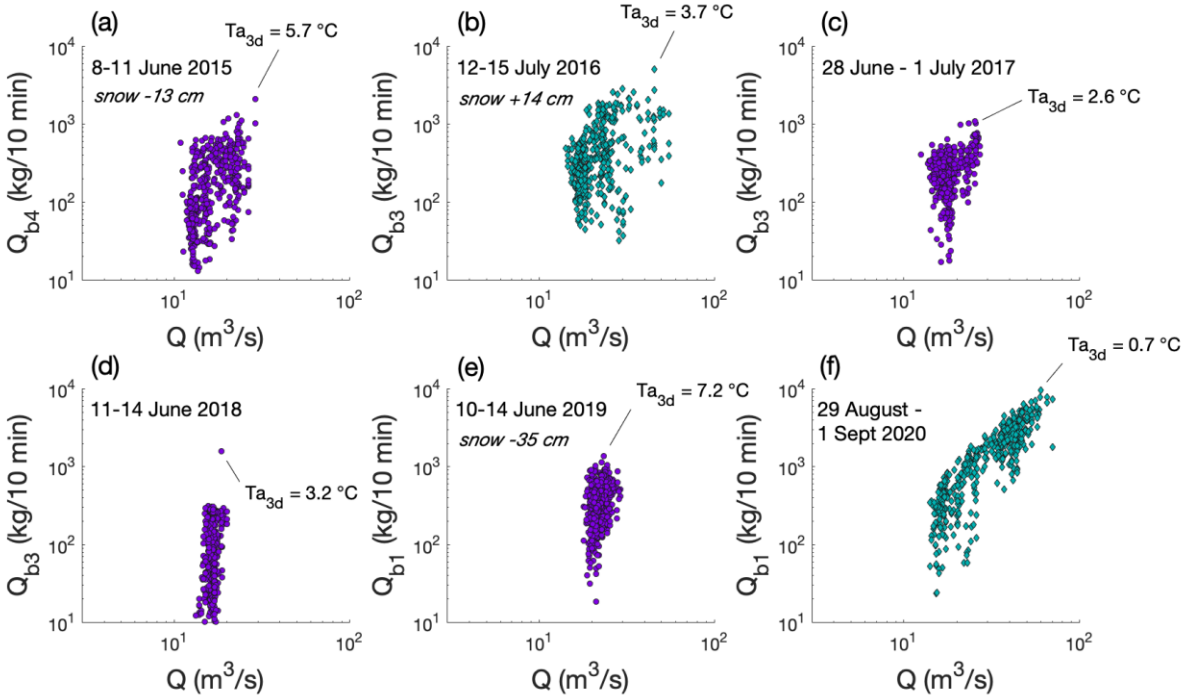

Figure 11 – Hysteresis cycles (counterclockwise) of the main flow event occurred from 2015 to 2020. Reported bedload rated are measured at one reference plate (plate 4 in 2015, plate 3 in 2016-2018, plate 1 in 2019-2020). The variation of snow height refers to the investigated period of time and when it is not indicated means absence of snow cover.

This complex interaction between hydrological and climatic parameters is confirmed by the analyses of the main bedload events occurred in the following years. In Figure 11, we show the scatter plots of bedload rates vs total discharge of the main bedload events occurred from 2015 to 2020. For each event, we report the mean air temperature Ta_{3d} at Madritsch AWS as well as the variation of snow height in the analyzed time windows, ranging from four to five days. The figure shows that bedload events occurring in June (Figure 11a, c, d and e) generally feature lower bedload peaks than events occurring from mid-July to August. Major bedload events, like the ones that occurred on 13 August 2014 and 29 August 2020, were triggered by large precipitation events (more than 50 mm of cumulated rainfall in 24 hours) occurring after warm summer days, and when the upper portion of the basin was mostly free from snow cover. On 29 August 2020 (Figure 11f) 8,100 ton of bedload were transported in 72 h, which correspond to the 70% of the annual transport.

4 Discussion

4.1 Advantages of using a power-based calibration equation

In the previous section, we showed how the bedload estimation performed with different signal metrics differ significantly. Evidence from the Sulden River indicates that the signal power is the most effective metric for representing the variability of bedload transport. The maximum amplitude underestimates annual bedload yield of about 50% compared to impulses. The explanation for this underestimation is that the raw signal sampled at 5 kHz exceeds the full scale (i.e., 10 V) during periods of intense transport. Consequently, the maximum amplitude is not representative of high bedload rates. Impulses underestimate bedload yield up to 20% and peak bedload rate of more than one order of magnitude. In fact, a too low impulse threshold leads to the damping of bedload peaks, which significantly contribute to the annual bedload yield during periods of intense coarse transport. This effect is well-visible comparing the bedload rate curves calculated with the signal power and different impulse equations (Figure 12). July 2016 is a month of intense bedload transport due to two flood events occurred on 12-15 and 29-31 July (Figure 12a). Adopting the impulse equation with threshold 0.01 V, the bedload peak of this latter event is damped by one order of magnitude (Figure 12b), producing an underestimation of the bedload yield of more than 50% for the whole month. The damping of the impulses does not occur during low-intensity transport periods (e.g., 16-20 July) when the signal fluctuates well below the clipping threshold (dashed line). Adopting impulse equations calculated with higher thresholds (0.04 V in Figure 12c and 0.16 V in Figure 12d) the clipping threshold progressively rises and the underestimation of the monthly bedload yield reduces. However, such higher thresholds are less sensitive to low-amplitude signals commonly generated during finer, lower-intensity bedload events, and thus may also lead to an underestimate of total bedload yields.
The bedload underestimation is the result of the well-known phenomenon of impulses saturation (Arattano et al., 2014), i.e. for high amplitude signal oscillations the number of impulses does not increase anymore once the clipping value is reached. The computation of signal power requires the raw signal to be saved and post-processed, but in most geophone-plate measuring station the raw signal is not stored and the impulses are calculated in real time in order to save disk storage space. In previous studies, it was argued that the similarity between the regression coefficients of impulses and signal power equations indicate that impulses are suitable to predict the transported bedload mass (Rickenmann et al., 2014). However, we believe that regression coefficients alone do not explain completely the process dynamics. In the field of debris-flow seismic detection, it is well-known that selecting a threshold that is too low can impede the correct representation of the different debris-flow surges and, on the other hand, choosing a higher threshold can result in the signal damping (Arattano et al., 2014). Here, we showed that the power of the geophone signal better represents the variability of the energy radiation produced by bedload transport. Thus, we think that the adoption of seismic parameters more representative of the physical phenomena – such as the signal power – should be preferred over impulses when the raw signal is available.

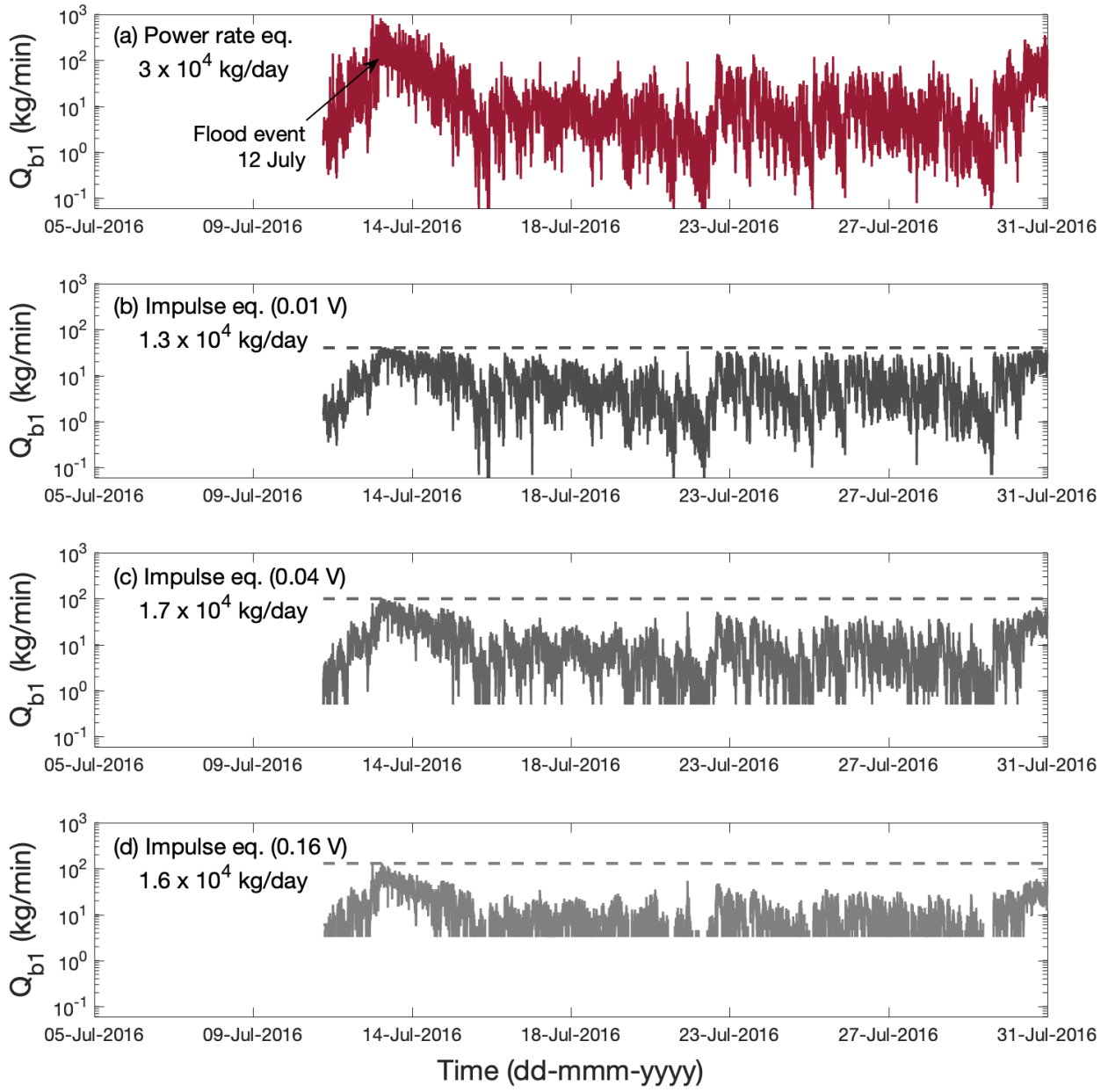

Figure 12 – Bedload rate (kg/min) at the plate 1 calculated by means of the signal power (a) and three impulse equations (b-c-d) during one month of intense transport (July 2016). The signal produced by the flood event of 12 July 2016 is damped in the impulse curves as it exceeds the clipping thresholds. Rising impulse thresholds, bedload peaks are better represented but the impulse curves are less sensitive to low-intensity signals: the lower cutoff limit (1 impulse) is 0.03 kg/min in (b), 0.5 kg/min in (c), and 3.25 kg/min in (d).

Moreover, we tried to explore possible relationships between the geophone signal and the bedload GSD. There is a positive correlation between the d90 of the direct bedload measurements and the signal power while the d50 does not show any significant correlation (see supplementary material). Vibrations produced by larger cobbles feature higher intensities and can dominate the seismic signal, as observed also in other catchments (e.g., Wyss et al., 2016). However, recent controlled flume experiments show how the increasing flow velocity reduces

the signal response using single grain sizes and the GSD variability of the transported bedload can influence the signal response of geophone plates (Nicollier et al., 2021). In addition, the signal response is influenced by the structure of the monitoring station, that is, number of plates and dimensions of both the steel frame and impact plates. Our findings show only a limited bedload coarsening for increasing water discharge within the sampled flow range, similarly to what observed in others mountain (Comiti et al., 2019; Rickenmann et al., 2012), and suggest that indirect seismic methods alone are probably not able to describe the GSD variability of bedload transport under natural conditions. This problem is most likely during intense transport periods, when many superimposed impacts from grains of different size occur at the same time. Indeed, the characteristics of single impacts are probably needed to infer more accurate information about bedload GSD by differentiating impacts from small and large clasts.

4.2 Factors controlling bedload rates and long-term yields

The analysis of continuous bedload data collected in the Sulden River highlights the complex interaction between hydro-meteorological parameters in controlling bedload variability. In steep mountain rivers, the maximum bedload rates are well constrained by the interplay of runoff, bed roughness, channel slope and channel geometry, while the actual bedload transport rates occurring during "ordinary" competent flows – i.e., excluding large, infrequent flood events – are limited by sediment supply (Comiti et al., 2019; Lane et al., 2017; Recking, 2012). In a glacier-fed river as the Sulden case, channel runoff is function of both hydrological (precipitation) and meteorological (air temperature, solar radiation) variables during the entire year, as snowmelt and glacier melt processes are driven by such variables (Engel et al., 2019a). However, different runoff origin (rainfall events, snowmelt, glacier melt) has been already associated to different bedload supply levels and thus extremely different bedload transport rates (Comiti et al., 2019; Mao et al., 2014). The latter authors embraced the use of bedload concentration to compare different periods featuring varying runoff origin (ice vs snowmelt contribution) and flow discharge. They found that in a small glacierized catchment (upper Saldur River, 20 km^2, 12% relative glacier area) bedload concentration during the glacier-melt period (10^1-10^2 kg m^{-3}) was several orders of magnitude higher than during snowmelt (10^{-4} - 10^{-2} kg m^{-3}). Such a marked difference in bedload concentration is not visible in the Sulden River (Figure 13), most probably because our data were collected at the basin outlet, where the drainage area is almost an order of magnitude larger than the upper Saldur. Indeed, bedload sources in the Sulden basin are numerous, covering relatively large areas (including the channels itself) and not only related to glacial and proglacial areas (Buter et al., 2020) as was instead the case for the Saldur River. Nonetheless, also in the Sulden River the median bedload concentration in July-August turns out to be higher than in May-June and September-October, respectively (Figure 13). The important contribution of glacial and proglacial sediments on bedload transport is supported by bedload sampling performed from 2015 to 2020 at the Sulden glacier snout (Engel et al., 2019b).

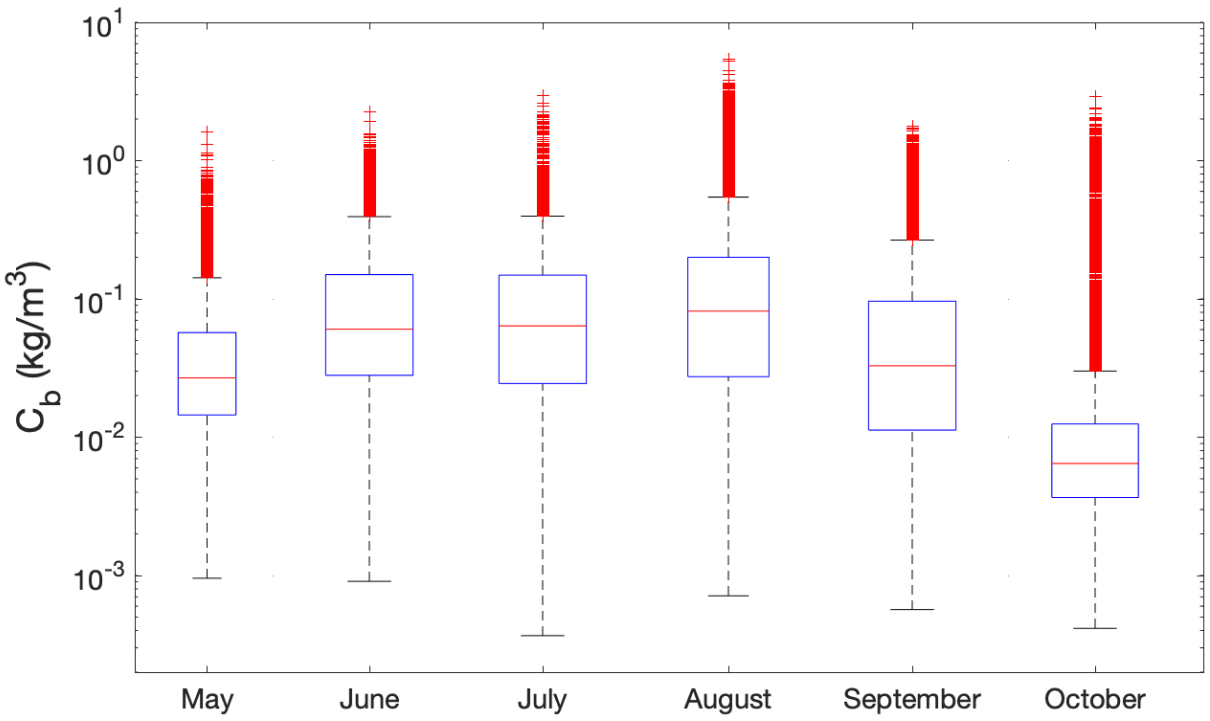

Figure 13 - Bedload concentration measured at the Stilfserbrücke station from 2014 to 2020 grouped.

Field evidence confirms that both glacial and proglacial sediment sources significantly contribute to the high bedload rate measured in the Sulden River in July and August, either during heatwaves or associated to intense rainfall events that occurred in the investigated period (Figure 14). In 2017, for example, a new glacier mouth opened and created a new proglacial stream that quickly eroded the glacial forefields (Figure 14b), thereby sharply augmenting bedload supply to downstream reaches (Buter, 2021). In the following years, the glacier retreated by about 200 m producing remarkable geomorphic changes in the proglacial drainage network and leaving abundant loose sediments readily available for transport (Figure 14c-f).

Despite large, rainfall-related floods can transport a disproportionate share of the annual bedload yield in some years (see section 3.2), glacier melt runoff appears to have a dominant role on the long-term bedload transport in the Sulden River. In fact, Figure 8 shows that the "most effective" discharge range for bedload (from about 18 to 20 $m^3 s^{-1}$) nicely corresponds to the values reached during the most intense glacier melt periods, with frequencies well higher – several times per year – than the 2-5 yr of recurrence interval found for a non-glacial mountain stream (i.e., at Rio Cordon, Lenzi et al., 2006). The role of ordinary (1-2 yr) and less frequent floods is also visible in Figure 8 (second and third peak of the E_b curve, respectively), but their contribution to the long-term bedload export from the Sulden basin is lower compared to the glacier-melt runoff peak. Such temperature-driven flow events will progressively lose their present dominance for bedload in the next decades as Sulden glaciers are rapidly retreating (Savi et al., 2021b). Then, rainfall-induced bedload events will become dominant, in agreement with what envisaged by some authors in the context of the ongoing climate warming (Antoniazza and Lane, 2021; Comiti et al., 2019; Li et al., 2021).

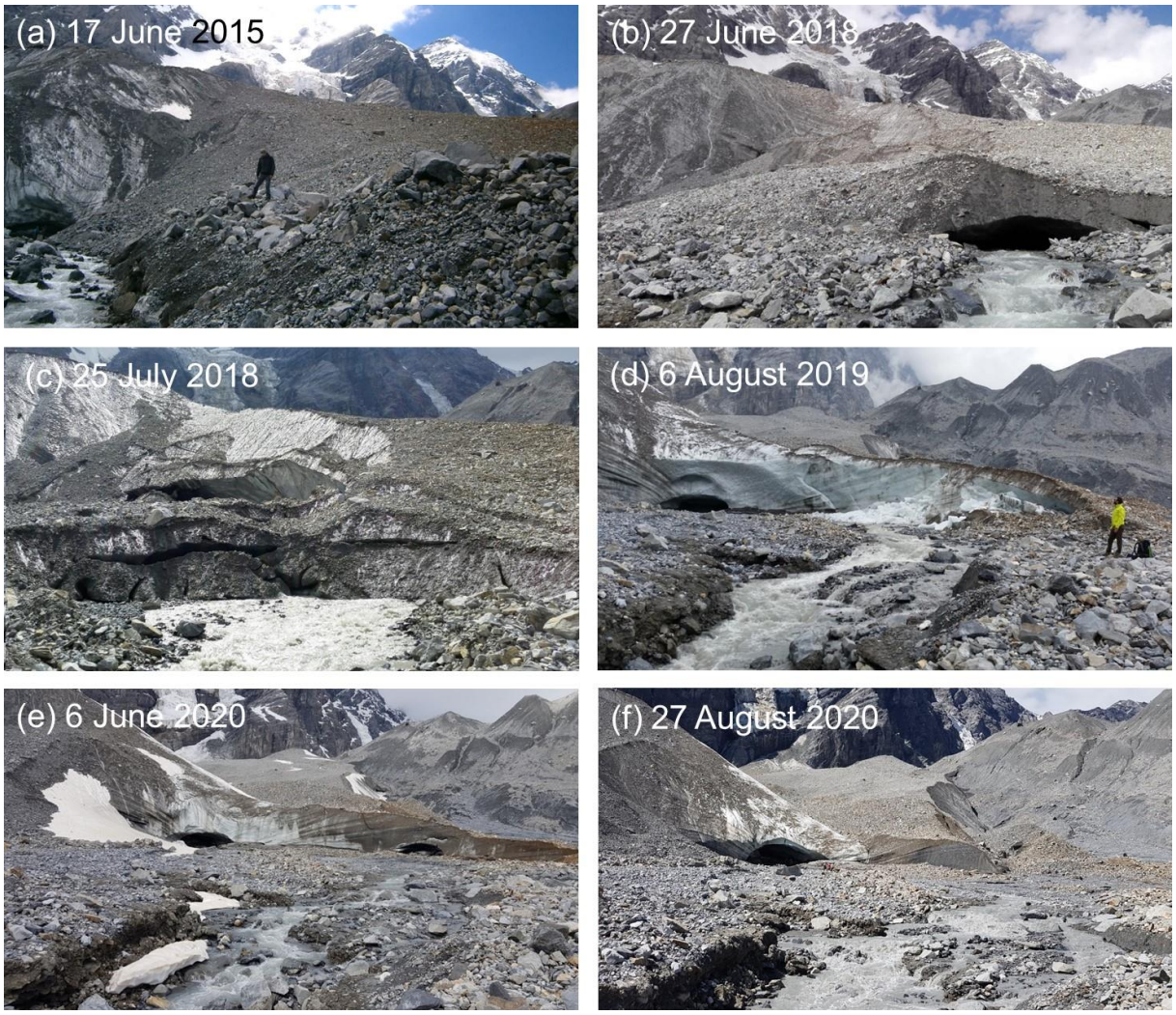

Figure 14 – Evolution of Sulden glacier front from 2015 to 2020, the location of the site is indicated in Figure 1.

The current strong control on bedload transport exerted by precipitation and air temperature is shown in Figure 15, where the whole bedload dataset collected from 2014 to 2020 is analyzed in comparison with hydro-meteorological parameters gathered at Madritsch AWS. In the figure, maximum bedload rates are classified based on the cumulated precipitation recorded in the previous 12 hours (P_{12h}) and on the mean air temperature of the previous three and seven days, respectively Ta_{3d} and Ta_w. This classification shows that:

- 50% of the total bedload yield occurs with zero precipitation in the previous 12 hours, highlighting the important role of the glacierized areas as sediment sources;
- the higher bedload rates (10^3 – 10^4 kg/10 min) and bedload concentration (5 kg m^{-3}) are associated to rainfall events occurred in the antecedent 12 hours (Figure 15b), indicating that largest bedload rates and concentration are reached when sediment sources from a vast part of the basin are connected to the outlet, as argued also by (Buter, 2021);
- most bedload transport is observed during snowmelt and glacier-melt periods. In particular, more than 95% of the total bedload yield occurs with Ta_{3d} > 0 °C (Figure 15c), whereas

about the 80% with Ta_w > 4 °C **(**Figure 15d). Also, in the flow interval 16-20 $m^3 s^{-1}$ (i.e., E_b peak), 95% of bedload transport occurs with Ta_{3d} > 0 °C and the 89% with Ta_w > 4 °C.

This analysis highlights the primary role of temperature in modulating glacier and snowmelt, thus driving most of the bedload transport, and the importance of intense rainfall events in generating peaks of sediment yield.

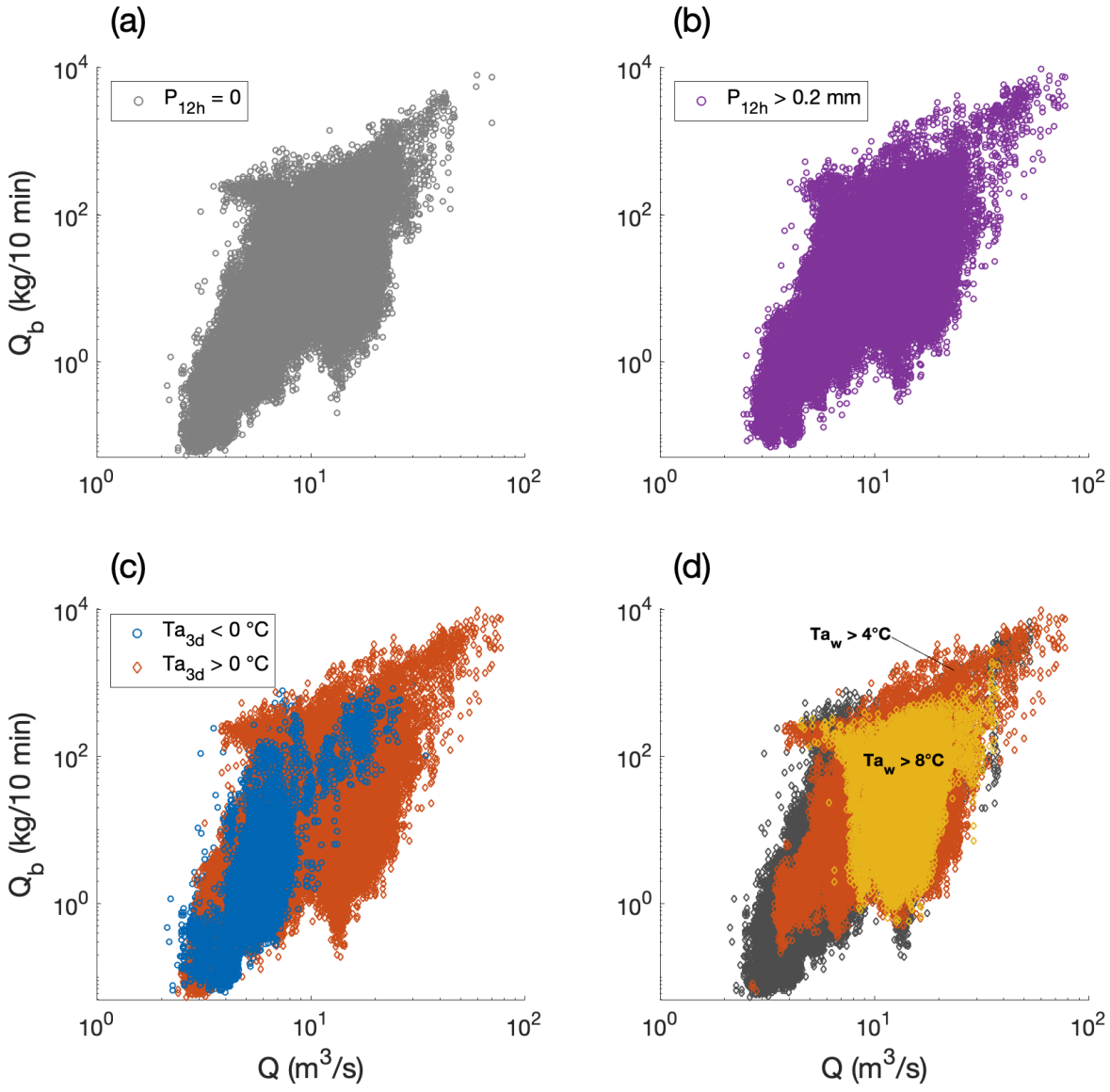

Figure 15 – Bedload rate at the reference plate vs the total discharge calculated on the whole monitored periods and classified using three hydro-meteorological parameters: the cumulated rainfall in the antecedent 24 hours (a and b), the mean air temperature of the previous 3 days (c) and the mean air temperature of the previous 7 days (d) measured at the Madritsch AWS.

5 Conclusions and perspectives

In this study, we presented an original geophone-plate dataset gathered in a glacier-fed Alpine river. We analyzed seven years of bedload data at different temporal scales. We propose the signal power as a more effective signal metric to represent peak bedload rates than threshold-based impulses, which can underestimate bedload yield by up to 20%. This allowed investigating the large variability of bedload rates and concentration observed at Sulden. We show how air temperature is useful to identify periods of intense bedload transport not only related to precipitation events but also to snowmelt and glacier melt. Bedload rate may vary up to four orders of magnitude for the same flow discharge and peak values are related to episodic summer rainstorm events superimposed on warm periods. Remarkably, the two largest flood events of the monitored period are associated with intense rainfalls and mobilized the 30% and the 70% of the annual bedload, respectively. Maximum values of bedload concentration are reached in July and August, highlighting the control exerted by glacier melt on bedload yield. The results of this study add an additional knowledge tile in the understanding of how climate may control the sediment dynamics of a glacierized basin. The future research at Sulden will address the bedload quantification at the glacier terminus and the identification of the relative contribution through time of the different sediment sources.

Acknowledgments

The research in the Sulden/Solda basin was supported by the AQUASED and GLORI projects (funded by the Autonomous Province of Bozen-Bolzano) and by the EFRE-FESR projects SEDIPLAN-i and -r. We are grateful to Roberto Dinale and Rudi Nadalet (Civil Protection Agency of the Autonomous Province of Bozen-Bolzano) and to the staff of the Meteorological and Hydrological Office of the Autonomous Province of Bozen-Bolzano for providing hydro-meteorological data. The design of the geophone-plate monitoring station of Stilfserbrücke - Ponte Stelvio benefited from advices by Dieter Rickenmann. We thank many colleagues and students for their support in bedload sampling activities in particular Ricardo Carrillo, Christian Kofler, Federica Minotti, Francesca Minute, Shusuke Miyata, Matteo Roverato and Vittoria Scorpio.

Open Research

A temporary private link to the geophone-plate dataset (2014-2020) employed in this study is provided in the supplementary material to support the peer review process. In the final paper, this link will be substituted with a persistent one to an Open Access data repository.

References

Antoniazza, G. and Lane, S. N.: Sediment yield over glacial cycles: A conceptual model, Prog. Phys. Geogr., doi:10.1177/0309133321997292, 2021.

Arattano, M., Abancó, C., Coviello, V. and Hürlimann, M.: Processing the ground vibration signal produced by debris flows: the methods of amplitude and impulses compared, Comput. Geosci., 73, 17–27, doi:10.1016/j.cageo.2014.08.005, 2014.

Autonomous Province of Bozen-Bolzano, U. I. e D.: Catasto dei ghiacciai dell'Alto Adige 2016/17., 2017.

Bagnold, R. A.: Bed load transport by natural rivers, Water Resour. Res., 13(2), 303–312, doi:10.1029/WR013i002p00303, 1977.

Barry, J. J., Buffington, J. M. and King, J. G.: A general power equation for predicting bed load

transport rates in gravel bed rivers, Water Resour. Res., 40(10), 1–22, doi:10.1029/2004WR003190, 2004.

Borga, M., Stoffel, M., Marchi, L., Marra, F. and Jakob, M.: Hydrogeomorphic response to extreme rainfall in headwater systems: Flash floods and debris flows, J. Hydrol., 518(PB), 194–205, doi:10.1016/j.jhydrol.2014.05.022, 2014.

Buter, A.: Geomorphic connectivity and dynamics in an Alpine glacierised basin under different scenarios., 2021.

Buter, A., Spitzer, A., Comiti, F. and Heckmann, T.: Geomorphology of the Sulden River basin (Italian Alps) with a focus on sediment connectivity, J. Maps, 16(2), 890–901, doi:10.1080/17445647.2020.1841036, 2020.

Carrivick, J. L. and Tweed, F. S.: Deglaciation controls on sediment yield: Towards capturing spatio-temporal variability, Earth-Science Rev., 221(June), 103809, doi:10.1016/j.earscirev.2021.103809, 2021.

Comiti, F. and Mao, L.: Recent Advances in the Dynamics of Steep Channels, Gravel-Bed Rivers Process. Tools, Environ., 351–377, doi:10.1002/9781119952497.ch26, 2012.

Comiti, F., Mao, L., Penna, D., Dell'Agnese, A., Engel, M., Rathburn, S. and Cavalli, M.: Glacier melt runoff controls bedload transport in Alpine catchments, Earth Planet. Sci. Lett., 520, 77–86, doi:10.1016/j.epsl.2019.05.031, 2019.

Coviello, V., Capra, L., Vázquez, R. and Márquez-Ramírez, V. H.: Seismic characterization of hyperconcentrated flows in a volcanic environment, Earth Surf. Process. Landforms, 43(10), 2219–2231, doi:10.1002/esp.4387, 2018.

Einstein, H. A.: The Bed-Load Function for Sediment Transportation in Open Channel Flows., 1950.

Engel, M., Penna, D., Bertoldi, G., Vignoli, G., Tirler, W. and Comiti, F.: Controls on spatial and temporal variability in streamflow and hydrochemistry in a glacierized catchment, Hydrol. Earth Syst. Sci., 23(4), 2041–2063, doi:10.5194/hess-23-2041-2019, 2019a.

Engel, M., Coviello, V., Andreoli, A. and Buter, A.: How does the presence of debris-cover on a glacier influence hydro-sedimentary dynamics? A comparison study from two proglacial streams in the Sulden catchment (Eastern Italian Alp s), in EGU General Assembly, vol. 21, pp. EGU2019-13295., 2019b.

Etzelmüller, B. and Frauenfelder, R.: Factors Controlling The Distribution of Mountain Permafrost in The Northern Hemisphere and Their Influence on Sediment Transfer Factors Controlling the Distribution of Mountain Permafrost in the Northern Hemisphere and Their Influence on Sediment Transfer, Arctic, Antactic Alp. Res., 41(1), 48–58, doi:10.1657/1938-4246(08-026), 2009.

Gimbert, F., Tsai, V. C. and Lamb, M. P.: A physical model for seismic noise generation by turbulent flow in rivers, J. Geophys. Res. Earth Surf., 119, 2209–2238, doi:10.1002/2014JF003201, 2014.

Habersack, H., Kreisler, A., Rindler, R., Aigner, J., Seitz, H., Liedermann, M. and Laronne, J. B.: Integrated automatic and continuous bedload monitoring in gravel bed rivers, Geomorphology, 291, 80–93, doi:10.1016/j.geomorph.2016.10.020, 2017.

Harrison, L. R., Legleiter, C. J., Wydzga, M. A. and Dunne, T.: Channel dynamics and habitat development in a meandering, gravel bed river, Water Resour. Res., 47, 1–21, doi:10.1029/2009WR008926, 2011.

Kofler, C., Mair, V., Gruber, S., Todisco, M. C., Nettleton, I., Steger, S., Zebisch, M., Schneiderbauer, S. and Comiti, F.: When do rock glacier fronts fail? Insights from two case studies in South Tyrol (Italian Alps), Earth Surf. Process. Landforms, 46(7), 1311–1327, doi:10.1002/ESP.5099, 2021.

Lane, S. N., Bakker, M., Gabbud, C., Micheletti, N. and Saugy, J.: Sediment export, transient landscape response and catchment-scale connectivity following rapid climate warming and Alpine glacier recession, Geomorphology, 277, 210–227, doi:10.1016/j.geomorph.2016.02.015, 2017.

Lenzi, M. A., Mao, L. and Comiti, F.: Magnitude-frequency analysis of bed load data in an Alpine boulder bed stream, Water Resour. Res., 40(7), 1–12, doi:10.1029/2003WR002961, 2004.

Lenzi, M. A., Mao, L. and Comiti, F.: Effective discharge for sediment transport in a mountain river: Computational approaches and geomorphic effectiveness, J. Hydrol., 326(1–4), 257–276, doi:10.1016/j.jhydrol.2005.10.031, 2006.

Li, D., Overeem, I., Kettner, A. J., Zhou, Y. and Lu, X.: Air Temperature Regulates Erodible Landscape, Water, and Sediment Fluxes in the Permafrost-Dominated Catchment on the Tibetan Plateau, Water Resour. Res., 57(2), 1–14, doi:10.1029/2020WR028193, 2021.

Mao, L.: The effect of hydrographs on bed load transport and bed sediment spatial arrangement, J. Geophys. Res., 117(July), 1–16, doi:10.1029/2012JF002428, 2012.

Mao, L., Dell'Agnese, A., Huincache, C., Penna, D., Engel, M., Niedrist, G. and Comiti, F.: Bedload hysteresis in a glacier-fed mountain river, Earth Surf. Process. Landforms, 39(7), 964–976, doi:10.1002/esp.3563, 2014.

Meyer-Peter, E. and Müller, R.: Formulas for Bed-Load transport, in IAHSR 2nd meeting, Stockholm, appendix 2, IAHR. [online] Available from: https://repository.tudelft.nl/islandora/object/uuid%3A4fda9b61-be28-4703-ab06-43cdc2a21bd7, 1948.

Nicollier, T., Rickenmann, D. and Hartlieb, A.: Field and flume measurements with the impact plate: Effect of bedload grain-size distribution on signal response, Earth Surf. Process. Landforms, 46(8), 1504–1520, doi:10.1002/esp.5117, 2021.

Raymond Pralong, M., Turowski, J. M., Rickenmann, D. and Zappa, M.: Climate change impacts on bedload transport in alpine drainage basins with hydropower exploitation, Earth Surf. Process. Landforms, 40, 1587–1599, doi:10.1002/esp.3737, 2015.

Recking, A.: Influence of sediment supply on mountain streams bedload transport, Geomorphology, 175–176, 139–150, doi:10.1016/j.geomorph.2012.07.005, 2012.

Rickenmann, D.: Comparison of bed load transport in torrents and gravel bed streams, Water Resour. Res., 37(12), 3295–3305, doi:10.1029/2001WR000319, 2001.

Rickenmann, D. and Fritschi, B.: Bedload transport measurements with impact plate geophones in two Austrian mountain streams (Fischbach and Ruetz): System calibration, grain size

691 estimation, and environmental signal pick-up, Earth Surf. Dyn., 5(4), 669–687,
692 doi:10.5194/esurf-5-669-2017, 2017.

693 Rickenmann, D., Turowski, J. M., Fritschi, B., Klaiber, A. and Ludwig, A.: Bedload transport
694 measurements at the Erlenbach stream with geophones and automated basket samplers, Earth
695 Surf. Process. Landforms, 37(9), 1000–1011, doi:10.1002/esp.3225, 2012.

696 Rickenmann, D., Turowski, J. M., Fritschi, B., Wyss, C. R., Laronne, J., Barzilai, R., Reid, I.,
697 Kreisler, A., Aigner, J., Seitz, H. and Habersack, H.: Bedload transport measurements with
698 impact plate geophones: Comparison of sensor calibration in different gravel-bed streams, Earth
699 Surf. Process. Landforms, 39(7), 928–942, doi:10.1002/esp.3499, 2014.

700 Rickenmann, D., Badoux, A. and Hunzinger, L.: Significance of sediment transport processes
701 during piedmont floods: The 2005 flood events in Switzerland, Earth Surf. Process. Landforms,
702 41(2), 224–230, doi:10.1002/esp.3835, 2016.

703 Rinaldi, M., Surian, N., Comiti, F. and Bussettini, M.: A methodological framework for
704 hydromorphological assessment, analysis and monitoring (IDRAIM) aimed at promoting
705 integrated river management, Geomorphology, 251, 122–136,
706 doi:10.1016/j.geomorph.2015.05.010, 2015.

707 Savi, S., Comiti, F. and Strecker, M. R.: Pronounced increase in slope instability linked to global
708 warming: A case study from the eastern European Alps, Earth Surf. Process. Landforms,
709 (February), 1–20, doi:10.1002/esp.5100, 2021a.

710 Savi, S., Dinale, R. and Comiti, F.: THE SULDEN/SOLDA GLACIER (EASTERN ITALIAN
711 ALPS): FLUCTUATIONS, DYNAMICS, AND TOPOGRAPHIC CONTROL OVER THE
712 LAST 200 YEARS, Geogr. Fis. Dinam. Quat., 44, 15–30, doi:10.4461/GFDQ.2021.44.2, 2021b.

713 Schneider, J. M., Rickenmann, D., Turowski, J. M., Schmid, B. and Kirchner, J. W.: Bed load
714 transport in a very steep mountain stream (Riedbach, Switzerland): Measurement and prediction,
715 Water Resour. Res., 52, 9522–9541, doi:10.1002/2016WR019308, 2016.

716 Turowski, J. M., Badoux, A. and Rickenmann, D.: Start and end of bedload transport in gravel-
717 bed streams, Geophys. Res. Lett., 38(4), 1–5, doi:10.1029/2010GL046558, 2011.

718 Turowski, J. M., Wyss, C. R. and Beer, A. R.: Grain size effects on energy delivery to the
719 streambed and links to bedrock erosion, Geophys. Res. Lett., 42, 1775–1780,
720 doi:10.1002/2015GL063159, 2015.

721 Vignoli, G., Simoni, S., Comiti, F., Agnese, A. D. and Bertoldi, W.: Monitoring sediment fluxes
722 in Alpine rivers: the AQUASED project, in Interpraevent, pp. 426–433., 2016.

723 Wolman, M. G. and Miller, J. P.: Magnitude and Frequency of Forces in Geomorphic Processes,
724 J. Geol., 68(1), 54–74, doi:10.1086/626637, 1960.

725 Wyss, C. R., Rickenmann, D., Fritschi, B., Turowski, J. M., Weitbrecht, V. and Boes, R. M.:
726 Laboratory flume experiments with the Swiss plate geophone bed load monitoring system: 1.
727 Impulse counts and particle size identification, Water Resour. Res., 52,
728 doi:10.1002/2015WR018555, 2016.

729

730 **Table 1.** Summary of the geophone plate dataset (2014-2020) analyzed in this paper: number of
731 days of complete recording available per plate and time windows of data gaps in the reference
732 period (between brackets).

733

	1 May – 31 Oct 2014	14 May – 30 Oct 2015	4 Jun – 31 Oct 2016	30 May – 27 Sep 2017	2 May – 31 Oct 2018	21 May – 28 Oct 2019	15 May – 10 Oct 2020
Plate 1	184	170	122 (13 Jun-11 Jul)	121	163 (12-31 Jul)	110 (18 Jun-31 Jul)	147
Plate 2	160 (7-30 Jun)	170	122 (13 Jun-11 Jul)	121	177 (13-18 Jul)	110 (18 Jun-31 Jul)	147
Plate 3	165 (12-30 Jun)	170	122 (13 Jun-11 Jul)	121	177 (13-18 Jul)	110 (18 Jun-31 Jul)	147
Plate 4	184	170	122 (13 Jun-11 Jul)	121	177 (13-18 Jul)	110 (18 Jun-31 Jul)	147
Plate 5	184	170	122 (13 Jun-11 Jul)	121	177 (13-18 Jul)	110 (18 Jun-31 Jul)	147
Plate 6	184	170	122 (13 Jun-11 Jul)	121	146 (13-18 Jul, 1-31 Oct)	110 (18 Jun-31 Jul)	147
Plate 7	154 (1-30 June)	170	122 (13 Jun-11 Jul)	121	155 (13-18 Jul, 3-24 Sep)	110 (18 Jun-31 Jul)	147
Plate 8	0	170	122 (13 Jun-11 Jul)	121	177 (13-18 Jul)	63 (18 Jun-31 Jul, 12 Sep on)	0

734

735 **Table 2.** List of direct bedload measurements performed by the portable trap from 2014 to 2020:
736 number of measurements (used for calibration after data cleaning), total bedload mass (d > 3.6
737 mm) extracted, reference plate of the direct measurements (plate number), d50 (daily mean
738 value) and water flow conditions (daily range) during measurements. Grain size data of the
739 bedload measurements performed in 2017 are not available (n.a.).

740

	Number of measurements	Sampled bedload mass (kg)	Reference plate	d50 (mm)	Water discharge (m^3/s)
5 June 2014	3 (2)	22.8	5, 6	11.3	7.7 – 7.8
6 August 2014	5 (4)	84.2	3, 4, 5, 6	19.7	19.7 – 20.1
9 September 2014	3 (2)	32.2	7	13	6.5 – 6.7
22 July 2015	6 (5)	353.6	5, 7	22	19.6 – 20.3
13 August 2015	9 (9)	395.6	1, 5, 6, 7	18.2	13.6 – 13.9
7 September 2017	9 (8)	100.5	1	n.a.	7.2 – 7.4
23 August 2018	5 (4)	182.3	1	14.2	14.3 – 14.5
7 August 2019	9 (9)	347.95	1, 2, 3, 4	14	21.1 – 21.2
25 June 2020	8 (6)	121.5	1, 3, 4, 5	10	12.8 – 14.1
22 July 2020	10 (8)	217.75	2	12.6	12.8 – 13.2
27 August 2020	8 (8)	208.2	1	16	9.2 – 11.8

741